Network subtypes of cortical similarity reveal molecular correlates of normative and compensatory ageing associated with longevity genes expression

Venia Batziou[1], Alexandra Young[2], Timothy Rittman[3], and Vesna Vuksanovic[1,✉]

[1]Health Data Science, Swansea University Medical School, Swansea, SA2 8PP, United Kingdom
[2]UCL Hawkes Institute and Department of Computer Science University College London, 90 High Holborn London WC1V 6LJ, UK
[3]Department of Clinical Neurosciences, University of Cambridge, Robinson Way, Cambridge, CA2 0SZ, UK

Ageing is marked by widespread cortical changes, but the molecular underpinning and network connectivity shaping this variability remain poorly understood. We analysed structural MRI from 952 adults aged 18–94 using morphometric similarity networks, subtype/stage inference, and cortical transcriptomics. Based on intra-network connectivity within three major cortical networks and their associations with longevity genes, two robust subtypes emerged. The *normative-ageing* subtype (metabolic-immune) showed connectivity profiles consistent with typical age-related decline and was enriched for genes involved in metabolism, insulin signalling, and immune regulation. The *compensatory* subtype (stress-repair) displayed more preserved intra-network connectivity and was linked to stress-response, DNA repair, and proteostasis genes. Although the two subtypes overlap in oxidative stress and neurodegeneration pathways, their distinct molecular signatures capture biologically meaningful differences in cortical ageing. By integrating network-based morphometry with transcriptomics, we establish a novel framework to distinguishes normative decline from compensatory adaptation in ageing profiles to provide biologically informed markers of brain ageing.

Keywords: | **brain ageing** | **morphometric similarity networks** | **cortical connectivity** | **longevity genes** | **subtype inference**

Correspondence: ***vesna.vuksanovic@swansea.ac.uk***

Introduction

Ageing is associated with widespread changes in brain structure and function, which unfold along similar, yet heterogeneous trajectories across individuals. Understanding the biological underpinnings of this variability is critical to differentiating healthy ageing from age-related neurodegenerative processes. While neuroimaging studies have delineated normative patterns of cortical morphometry – such as changes in cortical thickness, surface area, and folding (1–3) – the system-level organisation of these changes, and their relationship to molecular ageing mechanisms, remain elusive.

Morphometric similarity networks (MSNs) offer a biologically relevant, data-driven framework to investigate coordinated anatomical organisation across the cortex. MSNs take into account pairwise similarity of multiple morphometric features between cortical regions, providing a mesoscale map of structural connectivity that reflects underlying cytoarchitecture and shared developmental or genetic influences (4–6). Morphometric similarity is increasingly recognised as a biologically meaningful marker of individual differences in brain anatomy in both health (5, 7) and disease (8–10). The strong association between morphometric similarity and cortical cytoarchitecture suggests that MSNs capture coordinated cellular architecture (), enhancing their utility in ageing research. Furthermore, regions with higher morphometric similarity are more likely to be structurally and functionally connected (11, 12), making MSNs relevant for studying large-scale cognitive networks such as the default mode (DMN) and central executive network (CEN), which are especially sensitive to age-related reorganisation and cognitive decline (7, 13, 14).

Recent evidence suggests that MSNs variability is, at least in part, shaped by associations with genetic variations (15, 16), supporting their application in genetically informed models of inter-individual variability in brain ageing. Increasing evidence suggests that late-life psychiatric and cognitive disorders emerge from heterogeneous ageing trajectories shaped by metabolic, immune, and stress-response mechanisms, long before clinical symptoms become apparent (). Given their biological and functional relevance, MSNs may offer a robust framework to uncover the heterogeneity of cortical ageing trajectories, and to map them onto distinct molecular and network-level pathways. Here, we hypothesised that estimating individual variability in morphometric similarity profiles across the cortex could provide insights into how structural network organisation relates to heterogenous ageing patterns, and to both healthy and pathological trajectories of cognitive decline.

To address this, we utilised structural MRI, cortical transcriptomics, and normative modelling (incorporating the Subtype and Stage Inference (SuStaIn) framework (17)), to study MSN-functionally-based ageing phenotypes in over 900 healthy adults spanning the adult lifespan. Specifically, we applied a data-driven subtyping and staging approach to intra-network MSN connectivity within three core cognitive networks– the DMN, CEN, and visual network and examined

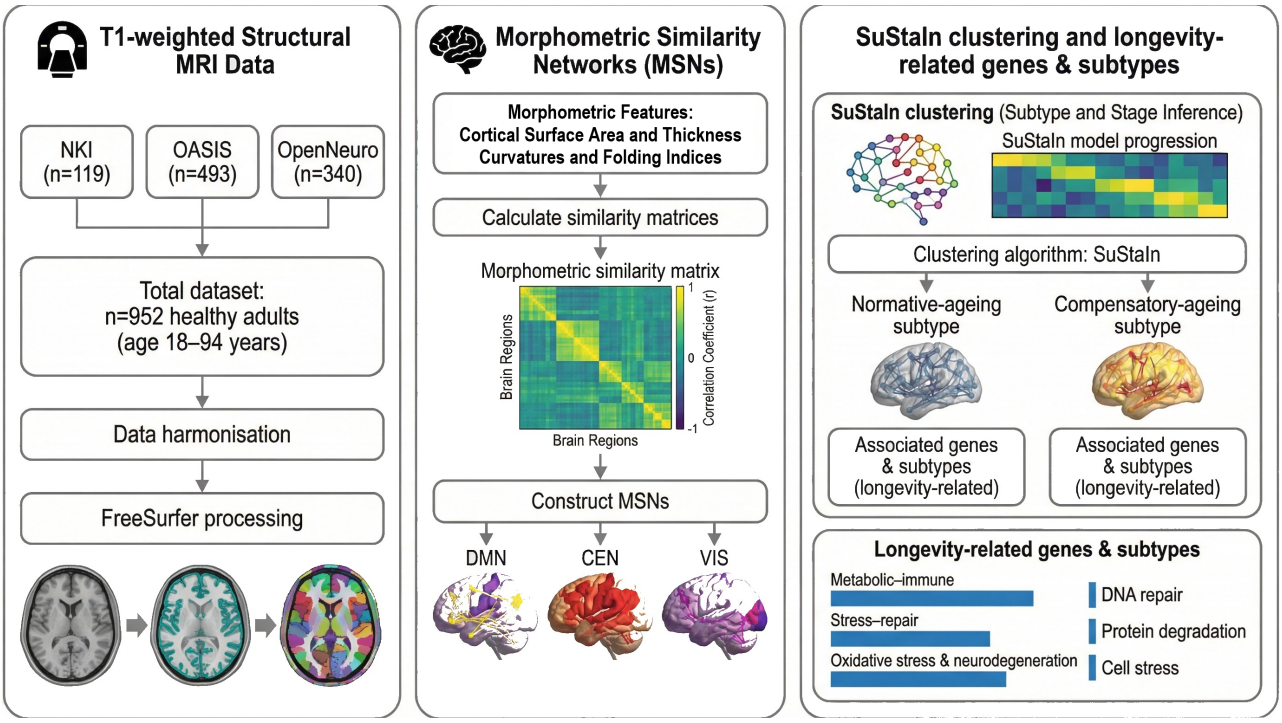

Fig. 1. Data analysis pipeline.

their spatial similarity with the cortical expression patterns of longevity-associated genes.

Materials and Methods

MRI datasets. MRI data included 952 healthy participants obtained from three MRI exchange platforms: The Nathan Kline Institute (NKI) (18), OASIS1-2 (19, 20) and IEEE-Openhb (21). All data were previously collected, and extensive documentations on the scanner types and protocols used for these studies can be found in (18–21). In short, only 3D-T1-weighted images from each dataset were used for the purpose of our study (see details in Supplementary Information section 1). All 952 images were preprocessed on the Swansea University High Performance Computer, using (FreeSurfer version 6.0) and the *recon-all* command with default parameters for cortical surface reconstruction.

Morphometric Similarity Networks Construction

The cortex was divided into 148 regions of the Destrieux Brain Atlas (DBA) implemented in FreeSurfer. DBA is parcellated by automatically classifying each vertex on the surface mesh as sulcal or gyral, which are then parcellated into 148 labels, i.e., 74 in each hemisphere. There are nine morphometric features of interest – surface area, gray volume, thickness average, thickness standard deviation, mean curvature, Gaussian curvature, folding index, curvature index – which can be extracted from the FreeSurfer output, for all 148 regions in the DBA. More detailed description of the procedure can be found in SI 1 and in (7).

The morphometric similarity networks (MSNs) were created by calculating the correlation coefficient of z-normalised morphometric features, to create 148×148 (matrices) networks for each participant. We then applied Fisher's transformation to convert the correlation coefficients to normally distributed z-scores. The self-correlations were replaced with the value 0. Three networks were created on combinations of different features for each participant: 4v-feature (4vf), 4c-feature (4cf) and 5-feature (5f), similar to (7). In short, the 4vf network was constructed on the inter- regional pairwise correlations between the volume, surface area, thickness, and thickness standard deviation. The 4cf networks were constructed by correlating intra-regional curvatures and their indices; 5-feature networks were construed on the intra-regional correlations between the volume, surface area, thickness, Gaussian curvature, and folding index, similar to (7). These feature combinations were chosen to capture complementary aspects of cortical morphology that differ in their sensitivity to ageing and developmental influences. The 4vf network combines volumetric and areal measures (volume, surface area, thickness, and thickness variability), which are known to decline with age and strongly reflect neurodegenerative and plastic processes (22). In contrast, the 4cf network, based on curvature-derived measures, represents geometric properties of cortical folding that are largely established early in development and relatively stable across adulthood (3). The 5f network integrates both volumetric and curvature-based metrics to provide a more comprehensive morphometric profile (5); however, this combination may dilute age-related variance by combining features with different biological timescales. Thus, examining all three configurations allows differentiation between structural features that are age-sensitive (4vf), developmentally constrained (4cf), and combined but less specific (5f), providing a more refined

assessment of which morphometric combination/dimension best capture ageing-related network (re)organisation.
We then calculated the weighted node degree (23) – to quantify connectivity characteristics within three cognitive networks: Default Mode Network, Central Executive Network and Visual Network (VIS). The mean value of the weighted node degree for each network's left and right hemisphere was used as a proxy for 'intra-network connectivity'. These networks are known to show distinct structural trajectories with ageing, with association networks such as the DMN and CEN exhibiting earlier and more pronounced morphometric changes than primary sensory systems like the VIS (24, 25). The DMN is associated with self-referential and memory-related processes; the CEN is involved in attention, working memory, and goal-directed control; and the VIS is supporting sensory-perceptual integration.

SuStaIn Model

For the SuStaIn model (17) we stratified the participants into two age groups – young adults (YA): 18 to 30 yea (n = 199) and healthy ageing group (HA): 45 to 94 yea (n = 753) (see Fig. S1 for their demographic characteristics). We normalised the MSNs to the YA group (17) and we then identified any (healthy ageing) biomarkers whose mean value were less than the mean value of the YA group (those biomarkers decreasing as ageing progresses) and multiply the data for these biomarkers by - 1. We selected z scores of 0.5, 1 and 1.5, and maximum z = 3. Only the ageing group is used for machine learning classification into subtypes. Given the balanced distribution of males and females in each group, the data were not corrected for sex at this stage. However, corrections for any potential confounds were applied during the post-hoc analyses and tests (see Statistical Analysis).

Genetic Analysis. Longevity-associated genes were obtained from the GenAge database and compared with cortical transcriptomics maps from the Allen Human Brain Atlas (AHBA). Only genes present in both datasets were retained for analysis. Regional expression values were mapped onto the DBA regions to match the MSNs resolution, similar to our eariler work (26). In cases where AHBA data did not cover a given cortical region, missing values were replaced with the regional or hemispheric mean. For each cortical region, partial correlations were computed between intra-network connectivity values (within DMN, CEN, VIS) and regional gene expression, while controlling for cortical thickness and surface area variations across parcelleted cortical regions. This framework, adapted from our previous work in a similar context (27), ensured that gene–network associations reflected regional variability beyond global morphometric variations. Multiple tests positive associations were corrected using False Discovery Rate (FDR) at the 0.05 level. For more details about the genetic analysis see SI section 1. Gene functions were obtained from RefSeq summaries in the NCBI Gene database National Center for Biotechnology Information (NCBI) and gene database Bethesda (MD): National Library of Medicine (US), National Center for Biotechnology Information, available here. A table generated from this search is available in the project's OFS directory (see SI for details).

Statistical Analysis

Study participants were divided into young adults (YA) and healthy ageing (HA) groups, according to their age band. Demographic characteristics of the participants for the YA and HA groups are shown in Table 1

Table 1. Demographic characteristics of the cohorts

Male/Female	97/102	320/433
Age range (years)	18 -30	45 - 94
Average age (years)	22(3)	66(11)

Cortical morphometric characteristics across the study groups were compared using the non-parametric Kruskall-Wallis test followed by the Mann-Whitney U test with the Bonferroni correction for post-hoc analysis. When data did not show mean differences between two classes, logistic linear regression was used to test for the effect of age and gender on subtypes classification. Associations between networks patterns and variations in the longevity genes' expressions in the brain were estimated using partial correlation, with cortical thickness and surface area as covariates. P values were FDR-corrected at a significance threshold of 0.05.
The overall data analysis pipeline is summarized in Fig. 1.

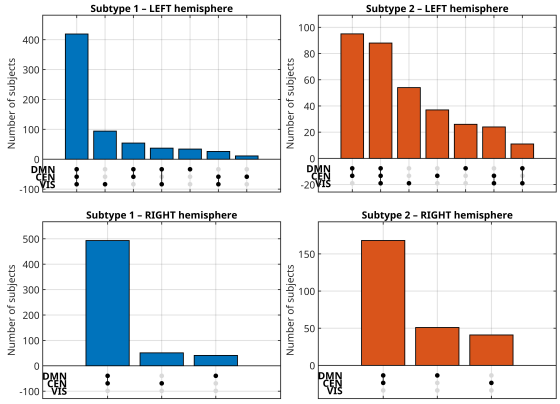

Fig. 2. Visualisation of subtype overlap across cortical networks (DMN, CEN, VIS) in left and right hemispheres. Bars represent the number of participants sharing each combination of subtype membership across the Default Mode (DMN), Central Executive (CEN), and Visual (VIS) networks. Filled dots indicate networks included in each overlap combination.

Results

Age-Associated Subtypes in Morphometric Similarity and Gene Expression. To investigate whether patterns of cortical network connectivity – measured by the intra-network node strength – show differences across the lifespan, we performed SuStaIn analysis on intra-network node strength calculated on the DMN, CEN, and VIS networks, using three types of MSNs – 5-feature, 4-volumetric-feature, and 4-curvature-feature. The analysis was performed separately for the left and right hemispheres to account for known

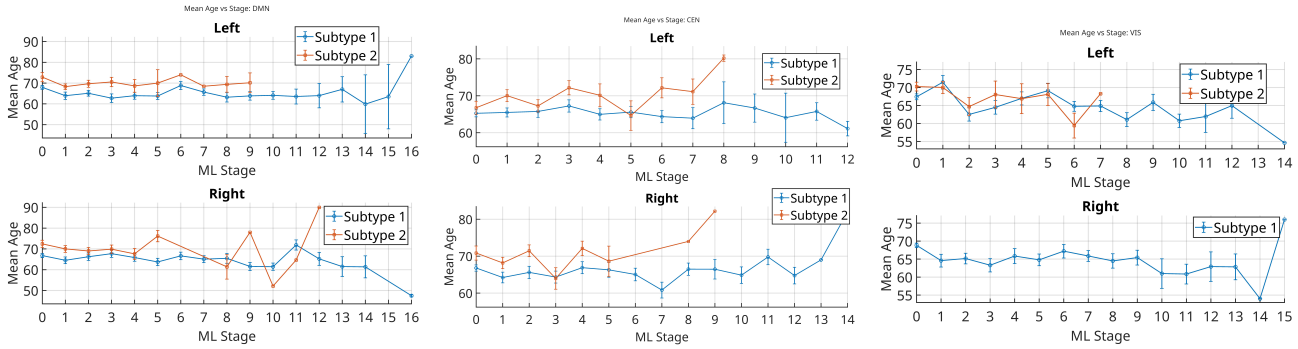

Fig. 3. Mean age across SuStaIn stages for Subtype 1 (normative) and Subtype 2 (compensatory) within the DMN, CEN and VIS (left to right panels) networks. Subtype 2 consistently shows higher mean ages than Subtype 1, across DMN and CEN intra-network connectivity, while in the VIS network, age differences were less pronounced. Across networks, higher SuStaIn stages corresponded to older mean ages, indicating age-related progression in intra-network connectivity. DMN - Default Mode Network; CEN - Central Network; VIS - Visual Network

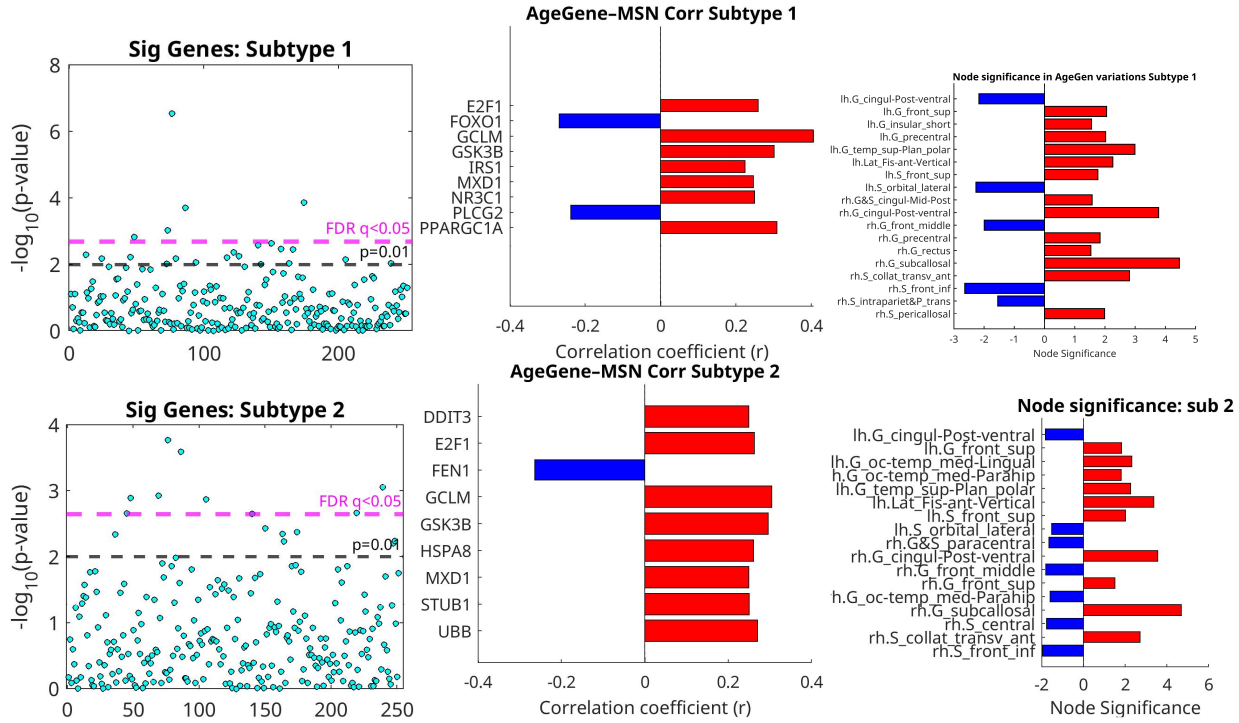

Fig. 4. Association between longevity-related gene expression and cortical morphometric similarity across ageing subtypes. (**Upper Panels**). Significant gene associations for Subtype 1 (**Lower Panels**) Significant gene associations for Subtype 2. Statistical significance is shown at an FDR-corrected threshold of 0.05 and an uncorrected threshold of 0.01, with associations controlled for regional variations in cortical thickness and surface area. Subtype 1 was enriched for genes involved in metabolic regulation and immune processes (e.g., IRS1, PPARGC1A, GSK3B, E2F1), with FOXO1 and PLCG2 showing negative associations suggestive of protective effects. Subtype 2 was characteried by stress- and neurodegeneration-related genes (e.g., DDIT3, UBB, STUB1, GSK3B), with FEN1 showing a negative association consistent with possible protection. Overlapping genes (E2F1, MXD1, GCLM, GSK3B) indicated shared pathways, but Subtype 2 showed stronger links to stress-response mechanisms, contrasting with the more metabolic/immune profile of Subtype 1. Regional contributions to molecular–network coupling in resilient and vulnerable ageing subtypes (right pannels). Bar plots show cortical regions with significant associations between intra-network morphometric similarity and longevity-genes-expression profiles.

hemispheric asymmetries in cortical structure, gene expression, and ageing trajectories (26, 28, 29). This separation allowed us to examine whether patterns of morphometric similarity and subtype emergence differ between hemispheres, providing a more anatomically and biologically precise characterisation of cortical changes across the lifespan. We found two distinct subtypes, denoted Subtype 1 and Subtype 2, emerging only within the 4vf type of MSNs. Subsequent gene-expression analyses revealed distinct molecular associations for each, enabling more intuitive, biological, interpretation as the *normative-ageing* and *compensatory* subtypes. In addition, the subtypes exhibited hemispheric asymmetry, i.e., a single subtype was found in the right hemisphere for the VIS network. This is consistent with the view that visual cortex regions are the last ones to experience age-related changes compared to, e.g., frontal or temporal regions (14, 30).

Fig. 2 shows the number of individuals within each subtype and their overlaps across the networks. Most of the time, individuals stay within their assigned sub-type and there is a strong consistency of over 80% of individuals classified into the same subtype regardless of the network examined. Mean age across SuStaIn *stages* for the subtypes, within the DMN, CEN and VIS (left to right panels) networks is showin in Fig. 3. Subtype 2 consistently shows higher mean values

than Subtype 1, across DMN and CEN intra-network connectivity, while in the VIS network, age differences were less pronounced. Across networks, higher SuStaIn stages corresponded to older mean ages, indicating age-related progression in intra-network connectivity.

Visualisations of the subtypes' associations with age is shown in Fig. S4. Both subtypes show that morphometric similarity increases with age across the DMN, CEN, and VIS. This pattern indicates that cortical regions within each network become more morphometrically 'similar' to one another with ageing, reflecting coordinated structural change with ageing. In addition, compensatory subtype (Subtype 2), has higher mean age compared to normative-ageing subtype (Subtype 1) (65.5 vs 70.0 years). However, they were not different on average. In the repeated test where age was included as a co-variate – the results showed significant ($p<.0001$) contribution of age to the sub-types' classification, reaching the accuracy of $\approx 93\%$ (see Fig. S2).

Associations between Network Subtypes and Longevity Genes. Having established two intra-network connectivity subtypes, we next investigated whether these distinct patterns of connectivity are associated with cortical maps of gene expression. In particular, we were interested in any significant associations between intra-network connectivity and human longevity genes (AgeGene) (31).

To examine the relationship between morphometric similarity and genes implicated in human longevity (31) (see also SI section 1 for detailed explanation), all age-gene–MSN associations were calculated using partial correlation, while controlling for regional variations in regional surface area and its thickness. Although a similar number of longevity-associated genes were significantly correlated with morphometric similarity across subtypes (Fig. 4), their spatial and network-level profiles differed. In Subtype 1, morphometric similarity was associated with expression of genes involved in, or related to metabolism, insulin signalling, and immune regulation. These included IRS1 and PPARGC1A (glucose/insulin pathways and cholesterol/obesity), GSK3B (energy metabolism and neurodegeneration), and transcriptional regulators (E2F1, MXD1). Notably, FOXO1 (myogenic growth, differentiation) and PLCG2 (immune signalling, autoinflammation) showed negative associations with intra-network connectivity, suggesting potential protective or resilience-related effects in this subtype. Subtype 2 was characterised by genes involved in cell stress, apoptosis, DNA repair, and protein degradation. These included DDIT3 (ER-stress–induced apoptosis), UBB (ubiquitin system, Alzheimer's/Down syndrome), STUB1 (protein quality control, spinocerebellar ataxia), and GSK3B (metabolic and neurodegeneration pathways). However, genes such FEN1, a key DNA repair gene, showed a negative association, indicating possible protective contributions against progression in this subtype. Despite overlaps (E2F1, MXD1, GCLM, GSK3B), Subtype 2 displayed stronger links to stress-response and neurodegenerative mechanisms. Overlapping genes (E2F1, MXD1, GCLM, GSK3B) mainly cluster around cell cycle regulation, oxidative stress, and metabolic/neurodegenerative pathways – suggesting a common core biology across both subtypes, with divergence in additional stress/apoptosis vs. metabolic/immune signatures. Unique to subtype 1 genes, involve metabolism, insulin signalling, mitochondrial function, and immune regulation, while genes unique to subtype 2 are related to cell stress responses, apoptosis, DNA repair, and protein degradation – processes closely tied to neurodegeneration [see, e.g., (32, 33)]. These findings suggest that although some neuroprotective pathways may be common across ageing subtypes, each group also exhibits distinct molecular signatures potentially reflective of different structural ageing trajectories associated with vulnerability or resilience to later-life cognitive impairment and possible to psychiatric disorders.

Pathway-wise, large-scale genomic analyses of brain and systemic ageing similarly report strong enrichment of lipid-metabolic and immune processes—along with drug-target associations, which conceptually align with the metabolic–insulin and immune signatures observed in our normative-ageing subtype (34, 35).

Longevity Genes and Subtype-specific Node Maps. To better understand the regional contributions to age-gene–MSN associations, we identified the top contributing cortical nodes for each subtype. There were 18 nodes for normative-ageing subtype 1 and 17 nodes for compensatory subtype (Subtype 2). Fig. 3 shows node significance in age-gene-MSNs associations, calculated on partial correlations corrected for variations in regional surface area and its thickness. Seven regions overlapped between subtypes, including bilateral posterior ventral cingulate, superior frontal gyrus, lateral orbital sulcus, and the right subcallosal gyrus – highlighting a shared involvement of core DMN regions. Interestingly, all of these overlapping nodes were located in the left hemisphere, suggesting a lateralised organisation of genetic contributions to network architecture. This left-hemispheric overlap was particularly prominent in regions affiliated with the DMN and CEN, (such as the left superior frontal gyrus, cingulate cortex, and lateral orbitofrontal areas). The predominance of left-sided overlap may reflect hemispheric specialisation in neurocognitive ageing processes, possibly related to verbal memory, executive control, or compensatory reorganisation.

The remaining nodes were subtype-specific. Normative-ageing subtype (Subtype 1) showed greater involvement of regions such as the left insula, precentral gyrus, and right intraparietal sulcus, involved in CEN and in sensorimotor domains. Compensatory subtype (Subtype 2) uniquely involved medial occipital and temporal regions including the lingual and parahippocampal gyri, suggesting stronger involvement of visual and memory-related circuits. Interestingly, only 3 Subtype 2 nodes were 'outside' of the DMN, CEN and VIS networks, in contrast to 6 of nodes of the Subtype 1. Also, 9 of 12 nodes affiliated with the three networks in Subtype 1 and 8 out of 14 in Subtype 2 were in the right hemisphere, suggesting again different involvement of genetic variations in network lateralisation.

Hemispheric distribution was balanced across subtypes (Sub-

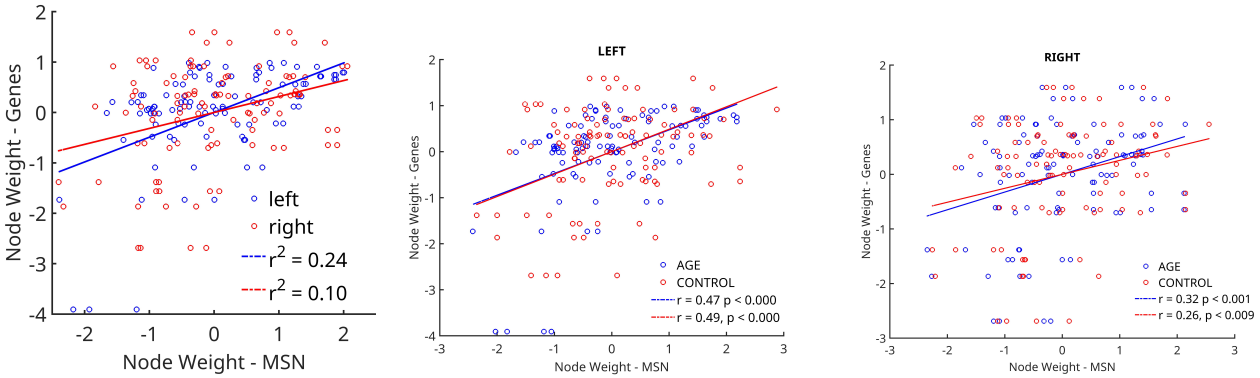

Fig. 5. Coupling between cortical network integrity and molecular gene-expression profiles. Scatter plots show the relationship between intra-network node weights derived from morphometric similarity networks (MSNs) and corresponding gene-expression network weights across cortical regions in the left (blue) and right (red) hemispheres. Solid lines indicate linear fits, with coefficients of determination (R^2) shown for each hemisphere. Positive associations indicate that regions with stronger network integration also exhibit higher expression of genes linked to ageing-related molecular pathways, with a stronger coupling observed in the left hemisphere. These results highlight hemispheric differences in the molecular embedding of cortical network organisation during ageing.

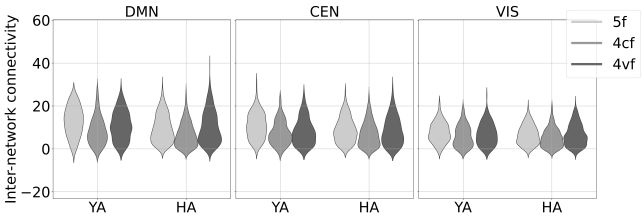

Fig. 6. The intra-network node strength for DMN, CEN and VIS networks in the two age groups: healthy young adults and healthy ageing (HA). Statistically significant differences were found between the YA and HA subjects for the 5-feature network in all three networks (DMN:p <0.0001; CEN: p <0.0001; VIS: p= 0.02), and for the 4-curvature-feature network in the DMN (p= 0.008). The p-values are corrected for multiple comparisons using Bonferroni correction.

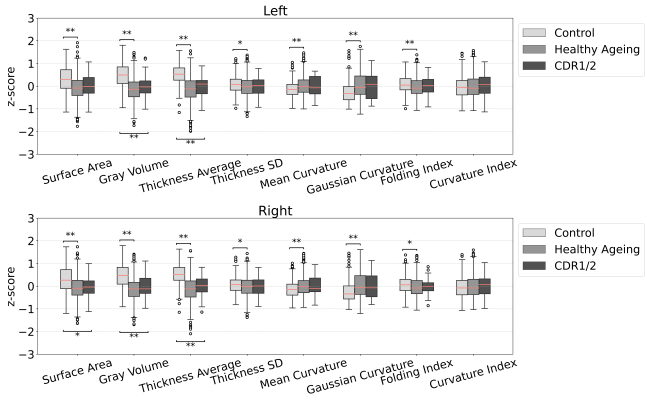

Fig. 7. Morphometric changes across cortical features in healthy young adults vs. older-age group, z-normalised to the feature mean. Mann-Whitney U test with Bonferroni correction. (**: p-value $<$ 0.001 *: p-value $<$ 0.01.) L = Left, R = Right hemisphere. YA = Young Adults, HA = Healthy Ageing

type 1: 8 left, 11 right; Subtype 2: 8 left, 9 right), with no clear lateralisation. Overall, while both subtypes were anchored in DMN architecture, normative ageing (Subtype 1) was more aligned with executive-motor integration, and compensatory subtype (Subtype 2) showed additional recruitment of visual and limbic regions. Our hypothesis is that preservation of visual network regions is a hallmark of resilience to cognitive impairment in later life.

To test the robustness of the age-gene–MSN associations, we re-ran the analyses without controlling for cortical thickness and surface area. The resulting set of significant genes was different (Fig. S3), suggesting that some associations may be driven primarily by global cortical morphology. Thus, our results corrected for the morphometric confounds (regional cortical thickness and surface area) more accurately reflect how regional morphometric similarity is associated with the longevity genes used in our analysis.

Genetic Associations with Bilateral Cortical Morphometric Networks. Finally, to explore the broader molecular underpinnings of cortical network organisation, we examined associations between bilateral MSNs and cortical gene-expression maps from the AHBA resampled to the DBA resolution. This analysis included all genes from the AHBA (mapped onto the DBA) to capture global transcriptional influences on cortical morphometric similarity beyond longevity-related pathways. The results revealed pronounced hemispheric asymmetry in gene–MSN associations, explaining 24% of variance in the left hemisphere and 10% in the right (Fig. 5). These associations were consistent across both age groups, suggesting that left-lateralised molecular-structural coupling represents a stable feature of cortical organisation across the adult lifespan.

Intra-network Connectivity and Ageing. Given that our age-related subtypes of intra-network connectivity were found only for 4vf MSNs, we next investigated whether intra-network connectivity differed between young adults and the healthy ageing group for 5v and 4cf MSNs. Intra-network node strength was calculated for the DMN, CEN, and VIS networks of the three different MSNs – 4vf, 4cf and 5v – and statistical differences were analysed between YA and HA groups.

Fig. 6 shows significant group differences in all three cognitive networks for the 5f network, and within DMN for the 4cf. This is in agreement with (5), where 5f MSNs were compared on the group-averaged level. Importantly, while the YA group showed clear differences between 5f and 4vf networks, these distinctions were absent in the HA group, suggesting a weakening of network-specific integration with age.

We then assessed broader morphometric changes across the cortex. Fig. 7 shows average morphometric features in YA

and HA groups. All features—except two curvature metrics—were significantly reduced in the HA group. These findings were consistent across bootstrapped analyses.

Relationship Between Subtypes and Cognitive Impairment. Finally, to contextualise the ageing-related subtypes, we compared HA subtypes to cognitively impaired individuals (n = 39) classified by the Clinical Dementia Rating scale (CDR=1 or 2). Figure 8 shows that, on average, the normative-ageing subtype (Subtype 1) exhibits intra-network morphometric similarity patterns that are simlar to those observed in the CDR 1/2 group, suggesting that both groups share comparable network-level structural changes typical of age-related decline. In contrast, the compensatory subtype (Subtype 2) shows a distinct profile, characterized by intra-network similarity patterns that diverge from both the normative-ageing and young adult groups. This difference suggests that compensatory reorganisation represents an alternative, adaptive mode of cortical ageing rather than a simple extension of normative structural change.

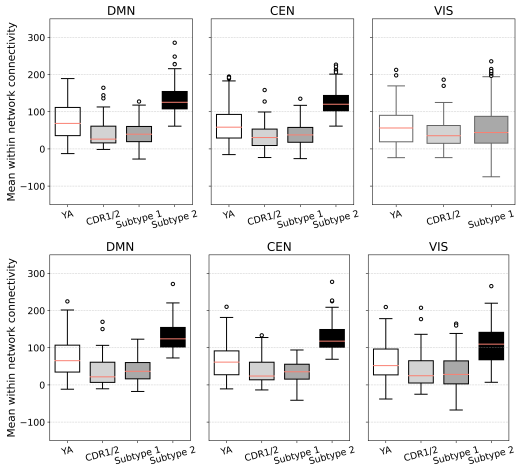

Fig. 8. Intra-network node strength for DMN, CEN and VIS networks in the mild to moderate cognitive impairment (CDR1/2), two subtypes of the healthy adult and in the young adult (YA) groups. Significant differences ($p<.001$) were found between subtype 2 and CDR1/2 in all boxplots where this subtype is present.

The CDR1/2 group's broader morphometric changes across the cortex are shown along the YA and HA groups (see Fig. 7).

Discussion

Here we present, to our knowledge, the first investigation of associations between longevity-related gene brain expression and morphometric similarity networks in a large adult cohort of over 900 individuals spanning the adult lifespan. The study design, of integrating morphometric similarity network analysis with cortical maps of longevity gene expression and normative modelling (incorporating subtyping and staging), provided a robust framework to capture individual variation in brain network organisation across adulthood. This approach revealed two distinct morphometric similarity subtypes, each characterised by unique as well as overlapping associations with cortical expression patterns of ageing-related genes. In addition, we linked these associations with involvement in core cognitive networks, including the default mode, central executive, and visual networks, and found evidence for network lateralisation, with overlapping gene-associated nodes primarily found within the left hemisphere. Based on their combined network and molecular associations, we refer to these as the normative-ageing and compensatory subtypes, reflecting distinct but complementary trajectories of cortical ageing.

Our results reveal two distinct age-related subtypes of intra-network morphometric similarity, emerging only from volumetric-feature-based MSNs (4vf) and present across core cognitive networks: DMN, CEN, and VIS (Figs. 2 & 3). These subtypes exhibited robust consistency across individuals and networks, as well as hemispheric asymmetries, particularly in the visual system. The presence of a single visual subtype in the right hemisphere aligns with prior evidence suggesting later vulnerability of the visual cortex to ageing compared to other association areas. The lack of such subtypes' classification from the 5f MSNs or curvature-only MSNs (4cf), indicates agreement of our results with the current view of the field. That is, that volumetric morphometric features are more sensitive to age-related network changes (see, e.g., (25)). The 5f MSNs, while comprehensive combination of features, may dilute ageing-relevant signals by combining feature types – age-sensitive volumetric measures and age-invariant curvatures – and the 4cf networks—focused solely on cortical folding—likely reflect more developmentally fixed aspects of brain structure that are less responsive to changes with ageing (for review see (36)). This highlights the specificity and sensitivity of volumetric metrics (regional surface area, thickness and volumes) in capturing biologically meaningful heterogeneity in cortical ageing.

Among our top findings is that these subtypes were differentially associated with cortical maps of longevity gene expression (Fig. 4). Subtype 1 showed spatial associations with genes involved in circadian regulation, glucocorticoid signalling, and metabolic processes—biological pathways broadly implicated in neuroendocrine ageing and resilience. Subtype 2 was associated with genes involved in DNA repair and proteostasis, reflecting a distinct molecular trajectory related to maintenance of genomic and proteomic integrity. Several genes, such as GCLM, DDIT3, and GSK3B, were shared across both subtypes, indicating common oxidative stress and apoptotic mechanisms that may underlie general ageing processes in the brain. Given their network characteristics shown in Fig. 8 – where Subtype 1 exhibits similarity to the cognitively impaired group and Subtype 2 shows higher intra-network connectivity than both young and healthy ageing groups – these molecular and network associations together motivate their more intuitive interpretation as the *normative-ageing* (Subtype 1) and *compensatory* (Subtype 2) subtypes.

Mapping these age-gene–MSN associations onto cortical regions revealed both subtype-specific and overlapping patterns (Fig. 3). While 18 nodes were significant in Subtype 1 (normative-ageing) and 17 in Subtype 2 (compen-

satory), seven regions – including posterior cingulate, superior frontal, and lateral orbitofrontal areas – were shared across subtypes. Importantly, all overlapping nodes were located in the left hemisphere, suggesting lateralised genetic contributions to brain network architecture in ageing. This hemispheric asymmetry was particularly evident within DMN and CEN regions, highlighting the role of lateralised cognitive systems, such as executive and verbal memory networks, in structuring molecular vulnerability or resilience ().

The remaining nodes displayed clear subtype specificity. Subtype 1 preferentially involved prefrontal and sensorimotor regions, while compensatory subtype prominently featured occipital and medial temporal areas, such as the parahippocampal and lingual gyri—regions associated with visual processing and memory. These patterns indicate that structural ageing subtypes are not only shaped by different molecular signatures but also target distinct neuroanatomical systems. The observed increases in intra-network morphometric similarity likely reflect convergent cortical changes rather than enhanced functional coupling. As regions within a network undergo parallel structural alterations, their morphometric profiles become increasingly correlated. Such network-level convergence could represent shared susceptibility to ageing processes or coordinated adaptation, depending on the underlying molecular context. In this framework, the normative-ageing subtype captures typical structural convergence with ageing, while the compensatory subtype exhibits more coordinated, possibly adaptive reorganisation consistent with stress-response and repair mechanisms. Our lateralisation analysis further supports this view: the left hemisphere showed stronger gene–MSN coupling (explaining 24% of variance) compared to the right ($\approx 10\%$) (Fig. 5). This asymmetry may reflect differential ageing dynamics across hemispheres and underscore the functional specialisation of cortical networks.

Finally, we contextualised these subtypes by comparing them to individuals with mild to moderate cognitive impairment (CDR1/2). The two cortical ageing subtypes revealed by our analyses capture distinct yet complementary trajectories of brain ageing. The normative-ageing subtype, although on average younger than the compensatory group, exhibited morphometric network profiles resembling those observed in individuals with early impairment, suggesting a trajectory characterized by more homogeneous structural change and typical age-related decline. This pattern was associated with the expression of longevity-related genes involved in metabolism, immune regulation, and neuroendocrine signalling (37–39). In contrast, the compensatory subtype showed greater intra-network similarity across association cortices and was enriched for genes supporting DNA repair and proteostasis, consistent with an adaptive, stress-response–driven pathway (40–42). Together, these findings indicate that age alone does not dictate the pattern of cortical ageing; rather, distinct molecular and network signatures underlie divergent paths of normative decline and compensatory adaptation. Although the present cohort consisted of cognitively unimpaired adults, the morphological resemblance between the normative-ageing subtype and the CDR 1/2 group suggests that coordinated structural change may precede overt cognitive symptoms, bridging normative and pathological ageing trajectories. his interpretation aligns with recent evidence that network-level alterations can emerge before amyloid or tau accumulation in Alzheimer's disease(43). In conclusion, our results reported here suggest existence of distinct network subtypes in morphometric similarity network organisation which are associated with specific genetic pathways revealing normative ageing and compensatory adaptation patterns over the lifespan. The integration of gene expression, morphometric similarity, and normative modelling provides a promising framework for tracking individual differences in ageing and may inform strategies for personalised ageing interventions or early detection of pathological trajectories. By spanning the adult lifespan, our study captures the full spectrum of cortical ageing trajectories – from early midlife to late adulthood – offering a unique opportunity to identify morphometric patterns that may serve as early biomarkers of network changes or compensatory mechanism. By combining normative modelling and transcriptomics, our findings pave the way for individualised models of brain ageing that are both biologically grounded and clinically informative.

Acknowledgements

This work was supported by the BRACE Charity Research Grant (DSR1085-100). V.B. was supported by this grant. A.Y. was funded by the Wellcome Trust (grant number 227341/Z/23/Z).

Author Contributions

Conceptualisation: V.V. (lead), T.R., and A.Y. Methodology: V.V., T.R., A.Y., and V.B. Formal Analysis: V.B. (image processing, SuStain, morphometric network analyses), V.V. (genetic analyses). Writing: Original Draft: V.V. (lead). Writing: Review and Editing: V.V., T.R., A.Y., and V.B. Supervision: V.V. (project lead and overall supervision).

Data and Code Availability

All data supporting the findings of this study are available from the corresponding author upon reasonable request. The full list of genes, along with derived morphometric similarity network (MSN) measures and subtype classification files, is available in the OSF repository folder associated with this study (link to be provided upon publication). Custom MATLAB scripts and processing workflows used for MSN computation and subtype analyses are also available in the same OSF repository.

Supplementary Note 1: Competing Interest Declaration

The authors do not have competing interests to declare.

1. Ivan Alvarez, Andrew J Parker, and Holly Bridge. Normative cerebral cortical thickness for human visual areas. *Neuroimage*, 201:116057, 2019.
2. Paul Allen, Helen Baldwin, Cali F Bartholomeusz, Michael WL Chee, Xiaogang Chen, Rebecca E Cooper, Lieuwe de Haan, Holly K Hamilton, Ying He, Wenche ten Velden Hegelstad, et al. Normative modeling of brain morphometry in clinical high risk for psychosis. *JAMA psychiatry*, 81(1):77–88, 2024.
3. Nagehan Demirci and Maria A Holland. Cortical thickness systematically varies with curvature and depth in healthy human brains. *Human Brain Mapping*, 43(6):2064–2084, 2022.
4. Lena Dorfschmidt, František Váša, Simon R White, Rafael Romero-García, Manfred G Kitzbichler, Aaron Alexander-Bloch, Matthew Cieslak, Kahini Mehta, Theodore D Satterthwaite, NSPN consortium, et al. Human adolescent brain similarity development is different for paralimbic versus neocortical zones. *Proceedings of the National Academy of Sciences*, 121(33):e2314074121, 2024.
5. Jakob Seidlitz, František Váša, Maxwell Shinn, Rafael Romero-Garcia, Kirstie J Whitaker, Petra E Vértes, Konrad Wagstyl, Paul Kirkpatrick Reardon, Liv Clasen, Siyuan Liu, et al. Morphometric similarity networks detect microscale cortical organization and predict inter-individual cognitive variation. *Neuron*, 97(1):231–247, 2018.
6. Jakob Seidlitz, Ajay Nadig, Siyuan Liu, Richard AI Bethlehem, Petra E Vértes, Sarah E Morgan, František Váša, Rafael Romero-Garcia, François M Lalonde, Liv S Clasen, et al. Transcriptomic and cellular decoding of regional brain vulnerability to neurogenetic disorders. *Nature communications*, 11(1):3358, 2020.
7. Vesna Vuksanović. Brain morphometric similarity and flexibility. *Cerebral Cortex Communications*, 3(3):tgac024, 2022.
8. Sarah E Morgan, Jakob Seidlitz, Kirstie J Whitaker, Rafael Romero-Garcia, Nicholas E Clifton, Cristina Scarpazza, Therese Van Amelsvoort, Machteld Marcelis, Jim Van Os, Gary Donohoe, et al. Cortical patterning of abnormal morphometric similarity in psychosis is associated with brain expression of schizophrenia-related genes. *Proceedings of the National Academy of Sciences*, 116(19):9604–9609, 2019.
9. Joost Janssen, Ana Guil Gallego, Covadonga Martínez Díaz-Caneja, Noemi Gonzalez Lois, Niels Janssen, Javier González-Peñas, Pedro Macias Gordaliza, Elizabeth Buimer, Neeltje van Haren, Celso Arango, et al. Heterogeneity of morphometric similarity networks in health and schizophrenia. *Schizophrenia*, 11(1):70, 2025.
10. Mario Tranfa, Maria Petracca, Marcello Moccia, Alessandra Scaravilli, Frederik Barkhof, Vincenzo Brescia Morra, Antonio Carotenuto, Sara Collorone, Andrea Elefante, Fabrizia Falco, et al. Conventional mri-based structural disconnection and morphometric similarity networks and their clinical correlates in multiple sclerosis. *Neurology*, 104(4):e213349, 2025.
11. Justine Y Hansen, Golia Shafiei, Jacob W Vogel, Kelly Smart, Carrie E Bearden, Martine Hoogman, Barbara Franke, Daan Van Rooij, Jan Buitelaar, Carrie R McDonald, et al. Local molecular and global connectomic contributions to cross-disorder cortical abnormalities. *Nature communications*, 13(1):4682, 2022.
12. Casey Paquola, Margaret Garber, Stefan Frässle, Jessica Royer, Yigu Zhou, Shahin Tavakol, Raul Rodriguez-Cruces, Donna Gift Cabalo, Sofie Valk, Simon B Eickhoff, et al. The architecture of the human default mode network explored through cytoarchitecture, wiring and signal flow. *Nature neuroscience*, 28(3):654–664, 2025.
13. Epifanio Bagarinao, Hirohisa Watanabe, Satoshi Maesawa, Daisuke Mori, Kazuhiro Hara, Kazuya Kawabata, Noritaka Yoneyama, Reiko Ohdake, Kazunori Imai, Michihito Masuda, et al. Reorganization of brain networks and its association with general cognitive performance over the adult lifespan. *Scientific Reports*, 9(1):1–15, 2019.
14. Roser Sala-Llonch, David Bartrés-Faz, and Carme Junqué. Reorganization of brain networks in aging: a review of functional connectivity studies. *Frontiers in psychology*, 6:663, 2015.
15. Andrew D Grotzinger, Travis T Mallard, Zhaowen Liu, Jakob Seidlitz, Tian Ge, and Jordan W Smoller. Multivariate genomic architecture of cortical thickness and surface area at multiple levels of analysis. *Nature Communications*, 14(1):946, 2023.
16. Dennis Van der Meer and Tobias Kaufmann. Mapping the genetic architecture of cortical morphology through neuroimaging: progress and perspectives. *Translational Psychiatry*, 12 (1):447, 2022.
17. Alexandra L Young, Razvan V Marinescu, Neil P Oxtoby, Martina Bocchetta, Keir Yong, Nicholas C Firth, David M Cash, David L Thomas, Katrina M Dick, Jorge Cardoso, et al. Uncovering the heterogeneity and temporal complexity of neurodegenerative diseases with subtype and stage inference. *Nature communications*, 9(1):4273, 2018.
18. Kate Brody Nooner, Stanley J Colcombe, Russell H Tobe, Maarten Mennes, Melissa M Benedict, Alexis L Moreno, Laura J Panek, Shaquanna Brown, Stephen T Zavitz, Qingyang Li, et al. The nki-rockland sample: a model for accelerating the pace of discovery science in psychiatry. *Frontiers in neuroscience*, 6:152, 2012.
19. Daniel S Marcus, Tracy H Wang, Jamie Parker, John G Csernansky, John C Morris, and Randy L Buckner. Open access series of imaging studies (oasis): cross-sectional mri data in young, middle aged, nondemented, and demented older adults. *Journal of cognitive neuroscience*, 19(9):1498–1507, 2007.
20. Daniel S Marcus, Anthony F Fotenos, John G Csernansky, John C Morris, and Randy L Buckner. Open access series of imaging studies: longitudinal mri data in nondemented and demented older adults. *Journal of cognitive neuroscience*, 22(12):2677–2684, 2010.
21. Benoit Dufumier, Antoine Grigis, Julie Victor, Corentin Ambroise, Vincent Frouin, and Edouard Duchesnay. OpenBHB: a Large-Scale Multi-Site Brain MRI Data-set for Age Prediction and Debiasing. *NeuroImage*, 2022.
22. Elizabeth R Sowell, Bradley S Peterson, Paul M Thompson, Suzanne E Welcome, Amy L Henkenius, and Arthur W Toga. Mapping cortical change across the human life span. *Nature neuroscience*, 6(3):309–315, 2003.
23. Mikail Rubinov and Olaf Sporns. Complex network measures of brain connectivity: uses and interpretations. *Neuroimage*, 52(3):1059–1069, 2010.
24. Anders M Fjell, Markus H Sneve, Håkon Grydeland, Andreas B Storsve, Inge K Amlien, Anastasia Yendiki, and Kristine B Walhovd. Relationship between structural and functional connectivity change across the adult lifespan: a longitudinal investigation. *Human brain mapping*, 38(1):561–573, 2017.
25. Christiane Jockwitz, Svenja Caspers, Silke Lux, Kerstin Jütten, Axel Schleicher, Simon B Eickhoff, Katrin Amunts, and Karl Zilles. Age-and function-related regional changes in cortical folding of the default mode network in older adults. *Brain Structure and Function*, 222 (1):83–99, 2017.
26. Nicolás Rubido, Gernot Riedel, and Vesna Vuksanović. Genetic basis of anatomical asymmetry and aberrant dynamic functional networks in alzheimer's disease. *Brain Communications*, 6(1):fcad320, 2024.
27. Vesna Vuksanović, Roger T Staff, Trevor Ahearn, Alison D Murray, and Claude M Wischik. Cortical thickness and surface area networks in healthy aging, alzheimer's disease and behavioral variant fronto-temporal dementia. *International journal of neural systems*, 29 (06):1850055, 2019.
28. Arthur W Toga and Paul M Thompson. Mapping brain asymmetry. *Nature Reviews Neuroscience*, 4(1):37–48, 2003.
29. Vyacheslav R Karolis, Maurizio Corbetta, and Michel Thiebaut de Schotten. The architecture of functional lateralisation and its relationship to callosal connectivity in the human brain. *Nature communications*, 10(1):1417, 2019.
30. Danielle J Tisserand, Jens C Pruessner, Ernesto J Sanz Arigita, Martin PJ van Boxtel, Alan C Evans, Jelle Jolles, and Harry BM Uylings. Regional frontal cortical volumes decrease differentially in aging: an mri study to compare volumetric approaches and voxel-based morphometry. *Neuroimage*, 17(2):657–669, 2002.
31. Robi Tacutu, Daniel Thornton, Emily Johnson, Arie Budovsky, Diogo Barardo, Thomas Craig, Eugene Diana, Gilad Lehmann, Dmitri Toren, Jingwei Wang, et al. Human ageing genomic resources: new and updated databases. *Nucleic acids research*, 46(D1):D1083–D1090, 2018.
32. Nuray Üremiş and Muhammed Mehdi Üremiş. Oxidative/nitrosative stress, apoptosis, and redox signaling: key players in neurodegenerative diseases. *Journal of Biochemical and Molecular Toxicology*, 39(1):e70133, 2025.
33. Elena Radi, Patrizia Formichi, Carla Battisti, and Antonio Federico. Apoptosis and oxidative stress in neurodegenerative diseases. *Journal of Alzheimer's disease*, 42(s3):S125–S152, 2014.
34. Daniel B Rosoff, Lucas A Mavromatis, Andrew S Bell, Josephin Wagner, Jeesun Jung, Riccardo E Marioni, George Davey Smith, Steve Horvath, and Falk W Lohoff. Multivariate genome-wide analysis of aging-related traits identifies novel loci and new drug targets for healthy aging. *Nature aging*, 3(8):1020–1035, 2023.
35. Philippe Jawinski, Helena Forstbach, Holger Kirsten, Frauke Beyer, Arno Villringer, A Veronica Witte, Markus Scholz, Stephan Ripke, and Sebastian Markett. Genome-wide analysis of brain age identifies 59 associated loci and unveils relationships with mental and physical health. *Nature Aging*, pages 1–18, 2025.
36. Karl Zilles, Nicola Palomero-Gallagher, and Katrin Amunts. Development of cortical folding during evolution and ontogeny. *Trends in neurosciences*, 36(5):275–284, 2013.
37. W Thomas Boyce, Pat Levitt, Fernando D Martinez, Bruce S McEwen, and Jack P Shonkoff. Genes, environments, and time: the biology of adversity and resilience. *Pediatrics*, 147(2): e20201651, 2021.
38. Mika Kivimäki, Alessandro Bartolomucci, and Ichiro Kawachi. The multiple roles of life stress in metabolic disorders. *Nature Reviews Endocrinology*, 19(1):10–27, 2023.
39. Joseph Bass. Circadian topology of metabolism. *Nature*, 491(7424):348–356, 2012.
40. Matías González-Quiroz, Alice Blondel, Alfredo Sagredo, Claudio Hetz, Eric Chevet, and Remy Pedeux. When endoplasmic reticulum proteostasis meets the dna damage response. *Trends in Cell Biology*, 30(11):881–891, 2020.
41. Mattia Poletto, Di Yang, Sally C Fletcher, Iolanda Vendrell, Roman Fischer, Arnaud J Legrand, and Grigory L Dianov. Modulation of proteostasis counteracts oxidative stress and affects dna base excision repair capacity in atm-deficient cells. *Nucleic acids research*, 45(17):10042–10055, 2017.
42. Gyujin Heo, Ying Xu, Erming Wang, Muhammad Ali, Hamilton Se-Hwee Oh, Patricia Moran-Losada, Federica Anastasi, Armand González Escalante, Raquel Puerta, Soomin Song, et al. Large-scale plasma proteomic profiling unveils diagnostic biomarkers and pathways for alzheimer's disease. *Nature Aging*, pages 1–18, 2025.
43. Julie Ottoy, Min Su Kang, Jazlynn Xiu Min Tan, Lyndon Boone, Reinder Vos de Wael, Boyong Park, Gleb Bezgin, Firoza Z Lussier, Tharick A Pascoal, Nesrine Rahmouni, et al. Tau follows principal axes of functional and structural brain organization in alzheimer's disease. *Nature communications*, 15(1):5031, 2024.
44. Anders M Dale, Bruce Fischl, and Martin I Sereno. Cortical surface-based analysis: I. segmentation and surface reconstruction. *Neuroimage*, 9(2):179–194, 1999.
45. Anderson M Winkler, Douglas N Greve, Knut J Bjuland, Thomas E Nichols, Mert R Sabuncu, Asta K Haberg, Jon Skranes, and Lars M Rimol. Joint analysis of cortical area and thickness as a replacement for the analysis of the volume of the cerebral cortex. *Cerebral cortex*, 28 (2):738–749, 2018.
46. Bruce Fischl and Anders M Dale. Measuring the thickness of the human cerebral cortex from magnetic resonance images. *Proceedings of the National Academy of Sciences*, 97 (20):11050–11055, 2000.
47. DC Van Essen and HA Drury. Structural and functional analyses of human cerebral cortex using a surface-based atlas. *Journal of Neuroscience*, 17(18):7079–7102, 1997.
48. Raymond Pomponio, Guray Erus, Mohamad Habes, Jimit Doshi, Dhivya Srinivasan, Elizabeth Mamourian, Vishnu Bashyam, Ilya M Nasrallah, Theodore D Satterthwaite, Yong Fan, et al. Harmonization of large mri datasets for the analysis of brain imaging patterns throughout the lifespan. *NeuroImage*, 208:116450, 2020.
49. Xiaosong He, Danielle S Bassett, Ganne Chaitanya, Michael R Sperling, Lauren Kozlowski, and Joseph I Tracy. Disrupted dynamic network reconfiguration of the language system in temporal lobe epilepsy. *Brain*, 141(5):1375–1389, 2018.

Supplementary information

Free Surfer Analysis and Output. All 952 images were preprocessed on the Swansea University High Performance Computer using FreeSurfer (version 6.0) and the *recon-all* command with default parameters for cortical surface reconstruction, ensuring consistency across different software and hardware versions. Additionally, MRI data were corrected for site-specific acquisition differences by including scanning site as a covariate in the analysis, which is a standard procedure followed in multisite studies.

In FreeSurfer, cortical surface area reconstruction is calculated by correcting intensity variations in MRI data, removing non-brain tissue (skull-stripping), segmenting the gray-white matter interface, and separating the hemispheres and subcortical structures. The resulting volume is then filled, giving a representation of the cortical surface. (44). Gray matter volume is calculated by forming an oblique truncated triangular pyramid between matching faces on the white and pial surfaces, which is then divided into three tetrahedra. The total volume the sum of the three tetrahedra (45). The thickness is computed as the average of the thickness between the gray/white boundary surface. The thickness standard deviation is computed based on the variation in these measurements across the vertices of the cortical surface within a specific region of interest (46). Mean cortical curvature is calculated as the average of the principal curvatures at each point on the cortical surface. Gaussian curvature is the product of the two principal curvatures. The folding index (FI) is computed by integrating the product of the maximum principal curvature and the difference between maximum and minimum curvature and dividing by 4p. The Curvature index represents the average amount of curvature per region (47). In short, FreeSurfer outputs were harmonised arccos datasets following recommendations on image processing and quality control from (48) and taking into account an improved inter-scanner segmentation stability of the FreeSurfer version 6.0, which was used here (49).

MRI Datasets. The Nathan Kline Institute (NKI) Rockland Sample: Anatomical T1-weighted MRI data were acquired using standard SIEMENS MAGNETOM Trio-Tim syngo MR B15 scanner using an MPRAGE sequence. The anatomical scan protocol is described in the following summary table (NKI-PROTOCOL). Structural images were collected using a three-dimensional high-resolution T1-weighted gradient-echo (MPRAGE) sequence [TR=2.5s, TE=3.5ms, flip angle=8 degrees, matrix size=256×256, voxel size=$(1\times1\times1\text{mm})^3$, 192 axial oblique slices]. Number of images preprocessed and used from this dataset was N = 119.

OASIS: Anatomical T1-weighted MRI data were acquired using a Siemens 1.5T Vision scanner using a Magnetization-Prepared Rapid Gradient Echo (MPRAGE) sequence. Structural images were collected using a three-dimensional high-resolution T1-weighted gradient-echo sequence with the following parameters: (TR): 9.7 ms (TE): 4.0 ms Flip Angle: 10°, Slices: 128 Resolution 256 × 256 (1 × 1 mm) (19). Number of images preprocessed and used from this dataset was N = 357 (OASIS-1) and N = 136 (OASIS-2). (There was 150 images in total in the OASIS-2 dataset, but 14 did not pass QC and were not included.)

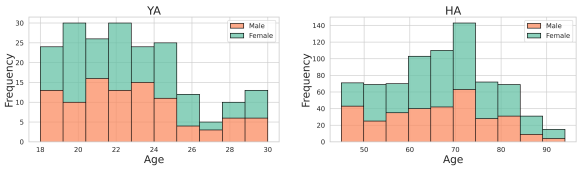

Fig. S1. Age histograms of young adults (YA) (n=199) (**Left Panel**) and healthy ageing(HA) group (n=753) (**Right Panel**).

IEEE: Anatomical T1-weighted MRI data in the Open BHB (Big Healthy Brains) dataset were aggregated from more than 70 acquisition sites across ten publicly available cohorts (e.g., ABIDE-1/2, CoRR, GSP, IXI, Localizer, MPI-Leipzig, NAR, NPC, RBP), encompassing over 5,000 unique healthy control participants (OPENBHB) (21). Number of images preprocessed and used from this dataset was N = 340.

Genetic Analysis Ageing genes were extracted from GenAge human ageing genes database, derived from the latest stable build of GenAge (31). The database, which consists of 307 age-related genes in total, was resampled to the variants that match those from the AHBA database. That way, 251 valid human genes were the same in both databases and the matched dataset was used in our longevity-gene-MSNs associations analysis. The full list of genes and their function, and related data files are publicly available in the project's OSF repository folder here.

DBA regional GWAS maps were extracted from the AHBA micro-array. In the instances where no a DBA region was mapped by the AHBA gene expression array – missing values were replaced with the corresponding overall mean – depending also on the statistical test performed on the maps (either individual or nodal).

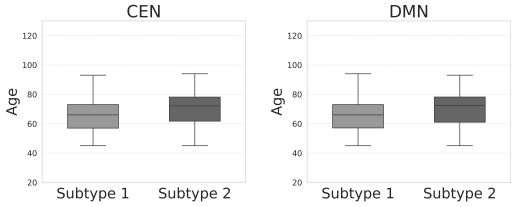

Fig. S2. Age boxplots of DMN and CEN of subjects' subtypes.

SuStaIn stages. Across all networks (DMN, CEN, VIS), SuStaIn stages showed age-related trends (see also Fig S5), with higher stages generally corresponding to older mean ages, supporting the model's sensitivity to age-related cortical progression. Subtype 2 (compensatory) consistently showed higher mean ages across stages compared to Subtype 1 (normative), particularly within the DMN and CEN networks. The age separation between subtypes was most pronounced in frontal and central networks (DMN, CEN), aligning with known vulnerability of these systems to ageing. In contrast, for inter-connectivity of the VIS network age differences between subtypes were less consistent, and

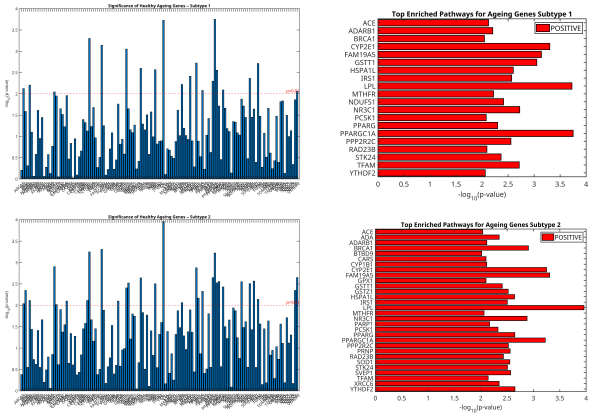

Fig. S3. association between longevity genes and cortical morphometric similarity. (**Top**). Subtype 1 and significant genes (**Right**) Subtype 2 and significant genes. The analysis was performed without corrections for cortical thickness and surface area variations.

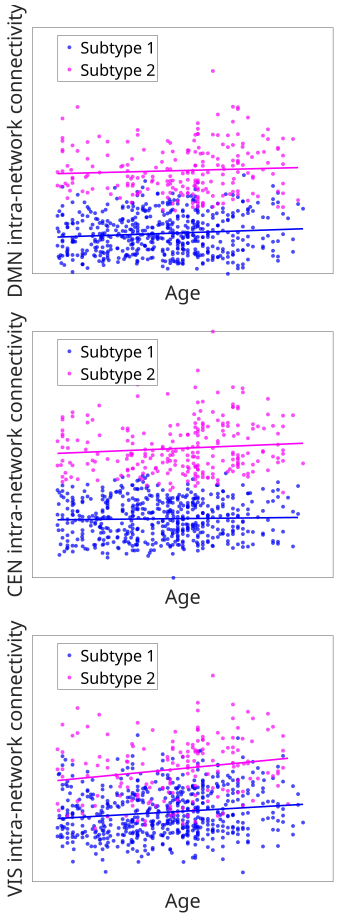

Fig. S4. Intra-network connectivity across the default mode (left), central executive (middle), and visual (right) networks as a function of age for two SuStaIn-derived ageing subtypes. Subtype 2 shows consistently higher connectivity than Subtype 1, suggesting a compensatory pattern of network organisation during ageing.

only Subtype 1 was evident in the right hemisphere.

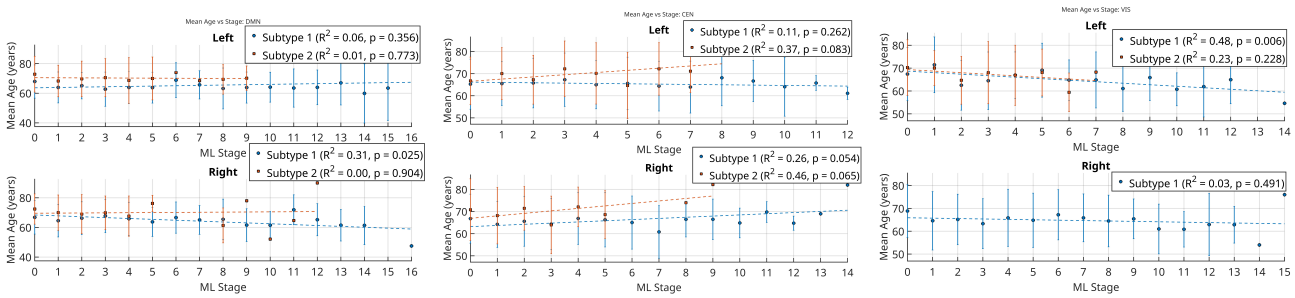

Fig. S5. Scatter plots showing mean age across SuStaIn stages for Subtype 1 (normative) and Subtype 2 (compensatory) in the left and right hemispheres of the DMN (top), CEN (middle), and VIS (bottom) networks. Dashed lines represent linear fits, with corresponding R^2 and p-values in the legends. DMN - Default Mode Network; CEN - Central Network; VIS - Visual Network